Journal of Materials Chemistry A

PAPER

View Article Online
View Journal

Cite this: DOI: 10.1039/c6ta10340e

Phosphonium plastic crystal salt alloyed with a sodium salt as a solid-state electrolyte for sodium devices: phase behaviour and electrochemical performance†

Faezeh Makhlooghiazad,*[a] Patrick C. Howlett,[a] Xiaoen Wang,[a] Matthias Hilder,[a] Douglas R. MacFarlane,[b] Michel Armand[a] and Maria Forsyth*[a]

Received 1st December 2016
Accepted 6th February 2017

DOI: 10.1039/c6ta10340e

rsc.li/materials-a

Mixtures of triisobutylmethylphosphonium bis(fluorosulfonyl)imide ($P_{1i444}FSI$) with different concentrations of NaFSI display composition-dependent phase behaviour with depression of the melting point upon NaFSI addition and suppression of crystallisation in the middle of the phase diagram and a higher-melting-point, NaFSI-rich mixed-phase region at compositions beyond 60 mol% NaFSI. Thermal treatment of the intermediate compositions results in complete crystallisation of the materials. All compositions showed high ionic conductivity (>10^{-5} S cm^{-1}) at 20 °C, and Na symmetric cells containing high concentration of NaFSI (Na|[$Na_{0.9}(P_{1i444})_{0.1}$]FSI|Na) were cycled efficiently at 50 and 90 °C at 0.05 and 0.1 mA cm^{-2}, respectively. Intermediate composition (Na|[$Na_{0.6}(P_{1i444})_{0.4}$]FSI|Na) cells were cycled at room temperature and 50 °C at 0.25 mA cm^{-2} with very low and stable cell polarisation (200 mV).

1. Introduction

Organic ionic plastic crystals (OIPCs) are a family of materials that have been receiving increasing attention as solid-state electrolytes. They are inherently non-flammable, non-volatile and alleviate leakage problems. Thus, they can improve the safety and reliability of a broad range of electrochemical energy devices. These materials can also possess high ionic conductivity, making them favourable materials for solid-state electrolyte applications.[1–19]

Adding a second salt component to the OIPC matrix is generally required for a specific device application. Moreover, mixing OIPCs with Li or Na salts (as required for Li or Na batteries) usually improves their ionic conductivity.[1,6,8,9,15,20–23] Possible conduction mechanisms in these materials have been discussed in several reports.[24–27] Previous research has focussed on the structural, physical and transport properties of OIPCs[5,26,28–36] and their electrochemical behaviour,[4,8,10,20,37,38] either in the neat OIPC or when mixed with a Li salt. Most of these studies have been undertaken on OIPCs with nitrogen-based cations such as pyrrolidinium,[5,22,26,28,31–35] imidazolium,[34] pyrazolium[20,39] and ammonium.[15,29,36] On the other hand, it has become increasingly clear that phosphonium-based OIPCs offer advantages such as higher conductivity and electrochemical stability compared to their nitrogen-based cation counterparts.[40–43]

Very recently an investigation of mixtures of a phosphonium OIPC ($P_{111i4}NTf_2$), containing the bis(trifluoromethanesulphonyl) amide (NTf_2) anion and the small trimethylisobutylphosphonium (P_{111i4}^+) cation and its corresponding sodium salt, has been reported. Their full phase diagram was determined and a new mixed compound was identified at a composition of 4 : 1 (*i.e.*, [$Na_{0.2}(P_{111i4})_{0.8}$]$NTf_2$).[44] Furthermore, electrochemical cycling and stability for two compositions were demonstrated in both the liquid and solid state of these mixtures.

FSI-based ionic liquids and OIPCs have also become of interest for Li and Na devices, where it is thought that the FSI anion may provide an improved solid electrolyte interphase (SEI) layer.[45–51] A full battery device based on Li|[$Li_{0.04}(P_{1i444})_{0.96}$]FSI|$LiFePO_4$ was also demonstrated with good capacity and excellent stability.[9] Whereas this electrolyte contained only 4 mol% LiFSI salt, more recent reports suggest that high salt concentrations are beneficial to the performance of Li- and Na-metal devices.[52]

The current work explores the phase behaviour and conductivity of $P_{1i444}FSI$/NaFSI mixtures across the entire composition range from 0 to 100 mol% NaFSI, using differential scanning calorimetry (DSC), scanning electron microscopy (SEM), energy-dispersive X-ray spectroscopy (EDX) and a.c. impedance techniques.

The sodium electrochemistry in 90 and 60 mol% NaFSI mixtures is also investigated using Na/Na symmetric cells to

[a]Deakin University Burwood Campus, Institute for Frontier Materials, 221 Burwood Highway, VIC 3125, Australia. E-mail: maria.forsyth@deakin.edu.au; fmakhlo@deakin.edu.au

[b]School of Chemistry, Monash University, Victoria 3800, Australia

† Electronic supplementary information (ESI) available. See DOI: 10.1039/c6ta10340e

evaluate the potential for these solid electrolytes to be used in sodium batteries. An additional benefit of this system compared to our previously reported system is the easier synthesis and greater availability of the P_{1i444} cation compared to P_{111i4} cation.

2. Experimental

2.1. Preparation of electrolytes

The triisobutylmethylphosphonium bis(fluorosulphonyl)imide (P_{1i444}FSI) OIPC was synthesized according to a previous report.[42] Particularly, triisobutylmethylphosphonium tosylate water solution (with 27.2 g, 0.07 mol of triisobutylmethylphosphonium tosylate) was mixed with KFSI solution (with 16.8 g, 0.077 mol, of KFSI) under magnetic stirring at room temperature. The formed white precipitate was collected by filtration and dissolved in 50 mL dichloromethane (DCM), then washed 5 times with deionized (DI) water in a separatory funnel. The final product was obtained by removing DCM using a rotatory evaporator and dried under vacuum on a Schlenk line at 50 °C for 3 days, which gave a water content less than 50 ppm (determined by Karl Fischer titration analysis). Sodium bis(fluorosulphonyl)imide (NaFSI) (99.99%) was purchased from Solvionic and used without further purification. Mixtures of P_{1i444}FSI/NaFSI containing various amounts of NaFSI were prepared inside an argon-atmosphere glove box. Homogenous solutions were obtained for lower concentrations of sodium salt by stirring and heating at 80 °C. For higher NaFSI concentration samples, distilled acetone was added to obtain a homogenous solution, and the acetone was then removed under high vacuum at 60 °C for 2 days. All samples were stored in sealed vials under an argon atmosphere inside the glove box. The chemical structure of P_{1i444}FSI is shown in Fig. 1.

2.2. Characterization

2.2.1. Thermal characterization. A Netzsch DSC 214 Polyma with liquid N_2 cooling, driven by Proteus 70 software, was used for thermal measurements. 5–10 mg samples were sealed in Al pans inside an argon-filled glove box. Typically, samples were cooled at 5 °C min^{-1} from room temperature to −100 °C and, after an isothermal equilibration time of 10 min, heated to 100 °C at the same scan rate. In some cases, a specific thermal cycling method was applied to crystallise the samples.

2.2.2. Electrochemical impedance spectroscopy (EIS). A Biologic MTZ-35 Analyser was used to evaluate solid- and liquid-state ionic conductivity of pure P_{1i444}FSI and NaFSI and their mixtures. Data was analysed with MT-Lab® software. EIS data was collected across a frequency range of 10 MHz to 0.1 Hz with a 100 mV amplitude and over a temperature range of −20 °C to 70 °C in 10 °C intervals. An equilibration time of 20 minutes was allowed at each temperature.

A Eurotherm 2204 temperature controller attached to the MTZ-35 was used to control the temperature automatically throughout the experiments. A thermocouple embedded in a brass block (that also contained a cavity to fit the dip cell) was used for temperature measurements.

Pre-dried pure OIPC mixed samples were placed inside a lab-designed dip cell equipped with two platinum wires protected by glass. The cell constant of the dip cell was calibrated from the known conductivity of 0.01 M KCl at 25 °C. Cell preparation was done inside the argon-filled glove box, and the dip cell was sealed hermetically. Regarding the pure NaFSI, firstly a pellet was made by pressing the powder in a sealed KBr die under 3 tonnes of pressure. Then the sample was dried at 50 °C in a vacuum oven for 24 hours. The dried pellet was placed between two stainless steel electrodes inside a lab-designed sealed barrel cell. The same analyser, frequency and temperature ranges were used for measuring the conductivity of pure NaFSI.

2.2.3. Scanning electron microscopy (SEM) and energy dispersive X-ray spectroscopy (EDX). SEM images and EDX maps were used to characterize the microstructures and morphologies of pure OIPC and the 90 mol% NaFSI mixture. Experiments were carried out on a JEOL JSM IT 300 Series SEM at accelerating voltages of 5 and 2 kV, equipped with an Oxford X-Max 50 mm^2 EDX detector. Samples were loaded onto carbon tape and sealed inside an Ar-filled canister in the glove box before being transferred to the SEM.

2.2.4. Symmetrical cell preparation. Microporous glass fiber separators (1.6 μm pore size and 260 μm thickness) were dried inside a vacuum oven at 100 °C overnight and then saturated with melted electrolyte. 9 mm diameter Na disc electrodes were punched out of Na metal (Sigma) that had been stored under paraffin oil (Merck Millipore), rolled and then mechanically cleaned in hexane using a brush. Symmetrical Na|Na CR2032 coin cells were prepared by assembling the Na discs and saturated separator in a Hohsen coin cell crimper, using a 0.5 mm spacer and a 1.4 mm spring. The whole cell assembly procedure was performed inside an argon-filled glove box. Cells were stored at 50 °C for 24 hours before being cycled on a Multi Potentiostat VMP3/Z (Bio-Logic) and data was collected using EC-lab software version 10.38.

Na symmetric cells containing either 90 mol% (an ultra-high concentration of NaFSI) or 60 mol% NaFSI in P_{1i444}FSI were cycled at 0.05, 0.1 and 0.25 mA cm^{-2} current densities at 90 °C, 50 °C and room temperature. The cut off voltage was set at ±5 V.

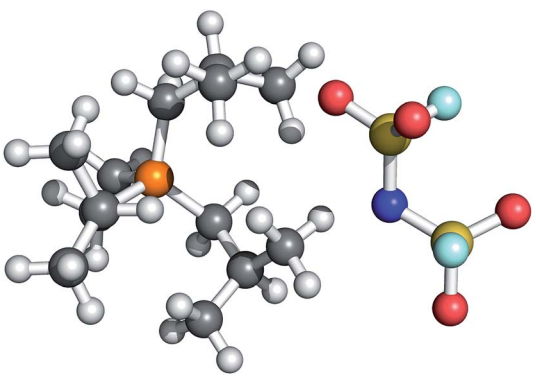

Fig. 1 Structures of $[P_{1i444}]^+$ (left) and $[FSI]^-$ (right).

3. Results and discussion

3.1. Thermal analysis and phase behaviour of $P_{1i444}FSI$, NaFSI and their mixtures

The DSC traces of the pure $P_{1i444}FSI$ and NaFSI salts and their binary mixtures at a range of concentrations from 0 mol% to 100 mol% NaFSI are presented in Fig. 2. The DSC heating trace of pure $P_{1i444}FSI$ shows three endothermic transitions which are assigned to two solid–solid phase transitions at 8 °C (the transition from ordered phase III to disordered solid crystalline phase II) and 24 °C (transition from phase II to more disordered phase I) typically seen in OIPC materials, and a melting transition at 37 °C with a low entropy of fusion (22 J mol^{-1} K^{-1}). This small entropy of melting is in agreement with Timmermans' criterion for molecular plastic crystals.[53] The observed solid–solid phase transitions result in rotational and orientational motion of the OIPC ions over the range of temperatures from 8 °C to 24 °C, as previously reported for this OIPC.[9]

The DSC trace for pure NaFSI shows a solid–solid phase transition at 90 °C before melting at 120 °C. This could suggest plasticity even in the neat NaFSI salt, which has not previously been reported to the best of our knowledge, and will be discussed later in the context of conductivity.

The phase behaviour of the binary systems changes significantly, as can be seen in Fig. 2. The melting transition is slightly depressed and the enthalpy of fusion decreases. This effect was observed previously in mixtures of OIPC with Na[33,38] or Li[9,23] salts and is typical for addition of a second component as a eutectic transition is approached.[44] In previous investigations, the lower enthalpy of melting in the mixed materials was related to the increasing presence of a liquid phase between the eutectic transition and the final melt or liquidus transition. Note that below the eutectic temperature the sample is completely solid, albeit as two solid phases. In the previous cases, an additional endothermic peak was always observed, and assigned to the eutectic temperature, T_E. However, an additional DSC peak was not observed in the present system, possibly because the peak overlapped a solid–solid phase transition.

To clearly observe the eutectic, the 5 mol% NaFSI sample was cycled between (−100 and 100 °C) very slowly, at a scan rate of 2 K min^{-1}. As shown in the inset to Fig. 2, the "transition" at 8 °C, is in fact composed of two peaks. We attribute this second peak to the eutectic transition, which occurs very close to the solid–solid phase transition as previously observed.[44]

Upon increasing the NaFSI salt concentration from 15 mol%, the phase behaviour changes dramatically, crystallisation transitions are seen during heating, along with a sharp decrease in melting point for the 20, 25 and 30 mol% NaFSI samples. Fig. 3a shows the crystallisation transition during heating before the melting transition, indicating that these samples do not freeze readily upon cooling. By applying an extended thermal cycling procedure this crystallisation peak disappeared and only the endothermic melting peak was observed (Fig. 3b) consistent with freezing of the sample during the thermal annealing steps. This means it is easy to supercool these samples and that they are very slow to reach their thermodynamically stable state; even a cooling rate of 5 K min^{-1} results in

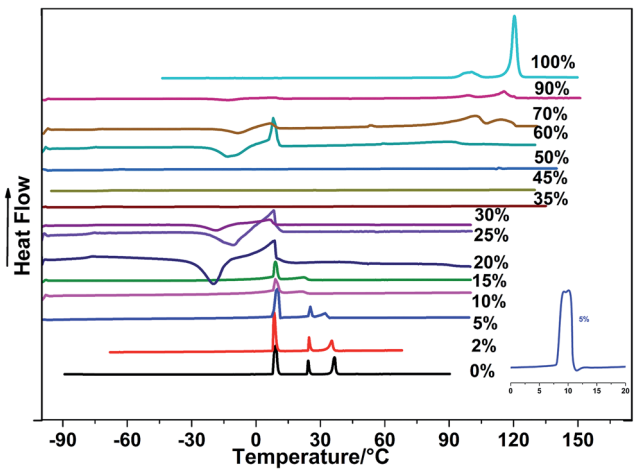

Fig. 2 DSC heating traces (5 K min^{-1}) of pure $P_{1i444}FSI$ and NaFSI and their mixtures. Inset is slower scan, 2 K min^{-1}.

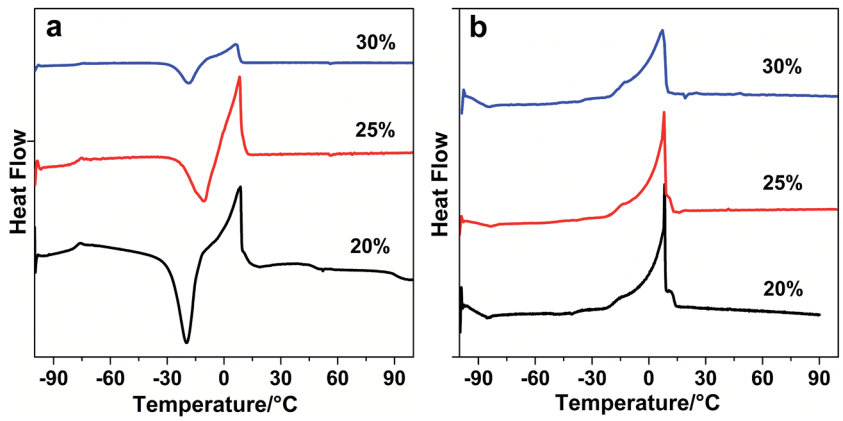

Fig. 3 (a) DSC heating traces of 20, 25 and 30 mol% NaFSI in $P_{1i444}FSI$ at scan rate of 2 K min^{-1}. (b) The samples were subjected to annealing at −10 and −30 °C (before and after crystallisation transition) for 1 hour at each temperature and cycled (−10, −30, −10, −30 °C) followed by cooling to −100 °C and heating to 100 °C.

some fraction of metastable phase. It should be noted that the endothermic transition in Fig. 3b emerged at the same temperature as the proposed eutectic transition (8 °C), thus confirming the assumption that the eutectic transition occurs at the same temperature as the solid–solid phase transition at 8 °C. Moreover, there is a very small peak near the eutectic peak at 20 and 25 mol% NaFSI that is reproducible and was not observed at 30 mol%. This suggests that this small peak is related to the final melting or liquidus transition of those samples. Given that for the 30 mol% sample the DSC heating trace shows only one peak, at the eutectic temperature (8 °C), it is likely that 30 mol% is the eutectic composition.

As the NaFSI concentration was increased from 30 to 60 mol%, the crystallisation process was completely suppressed. Fig. 4a shows that the system remains an ionic liquid, with a glass transition T_g observed around −75 °C. Such regions were reported previously in several electrolyte phase diagrams in which it was difficult to crystallise the materials, and are common in lithium-salt mixtures with OIPC.[54–57] The 40 and 50 mol% NaFSI samples were stored at −20 °C for one week then annealed under a specific thermal treatment (as described in Fig. 4 caption) to investigate if they would in fact crystallise. The DSC heating traces for 40 and 50 mol% NaFSI in Fig. 4 indicate an endothermic transition (once again exactly at the eutectic transition) and a final melting. This behaviour indicates that these mixtures have very slow crystallisation kinetics and can readily be supercooled; however the crystalline phase can be obtained by annealing at lower temperatures for some extended period.

Interestingly, by increasing the Na salt concentration ($x \geq 60$), a crystalline phase again appeared during cooling. The thermal phase behaviour of these compositions under specific thermal procedures is presented in Fig. 4b. This figure shows that the melting temperature increases with increasing NaFSI concentration. In addition, a solid–solid phase transition was observed in these samples at the same temperature as the solid–solid phase transition that was observed in the DSC heating trace of pure NaFSI. The 90 mol% NaFSI sample, as an example of an ultra-high concentration, was selected and its phase behaviour was studied over time. Fig. S1,† shows that the phase behaviour of the 90 mol% NaFSI sample changes significantly following a two week storage period in the glove box.

Thermal behaviour during the second heating cycle is also presented in Fig. 4c. Even after annealing the samples and applying a very slow cooling rate, only a glass transition was observed in the second traces. As illustrated in Fig. S2,† during

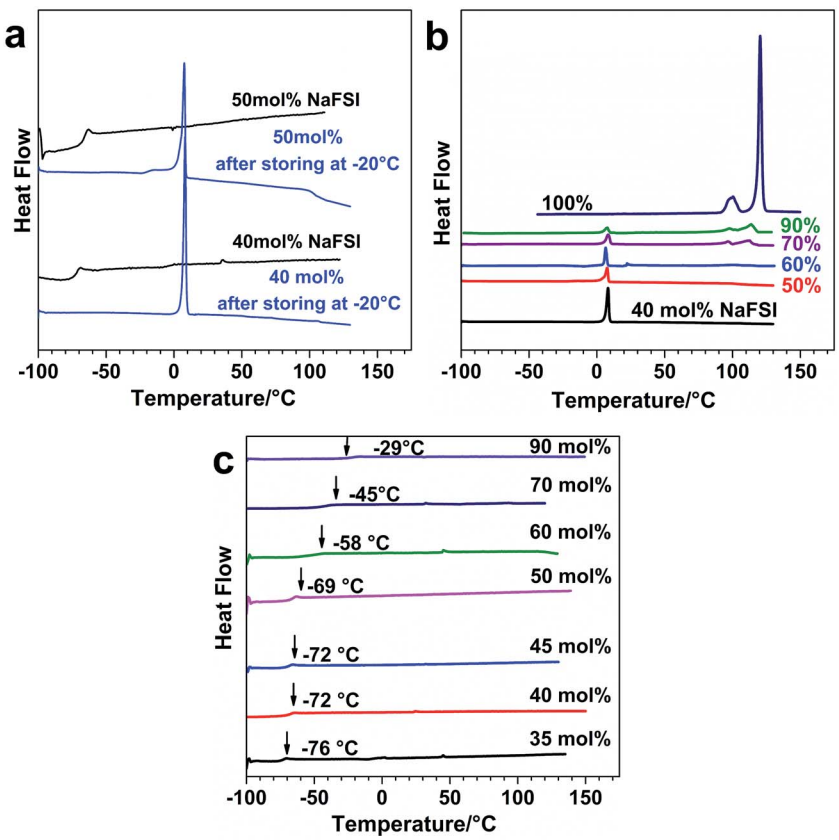

Fig. 4 (a) DSC heating traces of 40 and 50 mol% NaFSI after storing at room temperature inside glove box (black plots) and after storing at −20 °C and applying a thermal cycling procedure to induce crystallisation (blue plots). After storing the samples at −20 °C for one week, they annealed at −30, −40 and −50 °C for 2 hours at each temperature and cycled between −50 and −30 °C one time (−30, −40, −50, −30, −40, −50 °C) followed by cooling to −100 °C and heating to 100 °C. (b) Thermal phase behaviour of samples containing ≥40 mol% NaFSI. These samples annealed at −10 and −30 °C for 1 hour at each temperature and cycled (−10, −30, −10, −30 °C) followed by cooling to −100 °C and heated to 100 °C. (c) Second DSC heating traces of mixtures containing high contents of NaFSI.

the first cooling, the remaining liquid in the samples freezes into a crystalline phase; during the first heating the entire sample melts. This homogenous liquid is then cooled (during second cooling), but because the nucleation and growth kinetics for these mixtures are very sluggish, the liquid phase becomes a glassy solid, and a glass transition appears during the heating scan. The glass transition of all compositions shifts to higher temperatures upon increasing the NaFSI content (from −76 °C to −29 °C as shown in Fig. 4c). A partial phase diagram for this P_{1i444}FSI/NaFSI system is presented in Fig. S3.† Due to the complex metastable phase behaviour discussed above, the determination of the exact phase diagram remains a challenge.

3.2. Ionic conductivity behaviour in the P_{1i444}FSI/NaFSI binary

Ionic conductivity of pure P_{1i444}FSI and NaFSI and selected mixtures was determined and presented in Fig. 5. Three relatively small, but obvious, jumps in ionic conductivity are observed for the pure P_{1i444}FSI around the phase III to II (8 °C) and phase II to I (24 °C) transitions, as well as a large increase around the phase I to melt transition temperature. This behaviour agrees well with the DSC measurements.

Here the conduction mechanism is discussed for different regions in the phase diagram:

(I) OIPC rich region: (0 to 20 mol% NaFSI). Upon addition of 5 mol% NaFSI, the conductivity increases by 3 orders of magnitude and more than 3 orders of magnitude at 20 mol% at 20 °C. This sharp increase in conductivity suggests that the binary system has a different structure or phase behaviour from either of the pure salts. The higher conductivity above the eutectic temperature may also arise from the presence of a liquid fraction, according to the phase diagram (Fig. S3†). However, above 40 °C, where all samples are in the liquid state, the conductivity decreased slightly with increasing amount of NaFSI. This behaviour is expected for liquid systems in which conductivity depends on viscosity; the higher Na salt concentration leads to higher viscosity and consequently lower conductivity.[58–61]

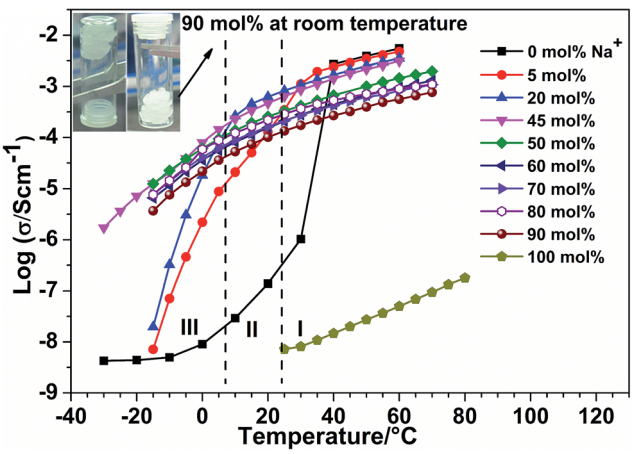

Fig. 5 Ionic conductivity of P_{1i444}FSI electrolytes for different concentrations of NaFSI.

(II) NaFSI-rich region: (60 to 90 mol% NaFSI). NaFSI-rich compositions show up to 3 orders of magnitude improvement in conductivity at 20 °C compared to the pure OIPC. According to the phase diagram this high conductivity may be due to the presence of the entrained Na-enriched liquid phase. We have previously suggested this liquid fraction occupies the intergranular space at the grain boundaries of the accompanying solid phase.[44] Thus the diffusion of ions will occur along these grain boundaries. It must be noted that these mixtures overall have a solid-like nature, despite the presence of a liquid phase (picture in Fig. 5). This is further supported by SEM/EDX measurements presented below and in Fig. S4.†

As discussed above, if 90 mol% NaFSI is allowed to equilibrate for two weeks at room temperature, the phase behaviour of this sample changes with an increasing amount of the stable crystalline phase forming. Fig. S5a† shows that the conductivity of the aged sample is significantly less than that of the as-prepared sample. Furthermore, a small jump in conductivity of the two-week aged sample appears at the eutectic transition (8 °C). This finding is consistent with the DSC results discussed above.

The ionic conductivity for the 90 mol% NaFSI sample was monitored over 40 days at 50 °C (Fig. S5b†). More than one order of magnitude decrease in conductivity was observed during this time, after which it remained relatively stable above 10^{-5} S cm^{-1}.

3.3. Morphology (energy dispersive X-ray spectroscopy (EDX))

SEM-EDX was used to study the distribution of elements throughout the 90 mol% NaFSI sample. N, O, F and S were all detected with high intensity, as expected, because of the FSI anion in both OIPC and NaFSI (Fig. 6a). On the other hand the P and C contents were low, as expected, because the sample contained only 10 mol% of the phosphonium (P_{1i444}^{+})-based OIPC. EDX images in Fig. 6b show that the FSI anion is distributed evenly throughout the sample. As both salts contain the FSI anion, both the liquid- and solid-state phases will contain N, O, F and S. The Na element also appears to be relatively uniformly distributed throughout the sample although there is less intensity in regions where there is high carbon. Fig. 7 shows the EDXs maps for C, which is only present in the P_{1i444} component of this material, and indicates that this cation appears only in some regions, consistent with the liquid phase evident in the SEM.

3.4. Electrochemical behaviour

3.4.1. Galvanostatic cycling of Na|[$Na_x(P_{1i444})_{1-x}$]FSI|Na symmetrical cells. Na symmetric electrochemical cells were constructed to investigate the stability of the electrolytes, as well as the redox behaviour of the sodium species and the possibility of reversible Na-metal deposition and dissolution in these materials. These cells can also be used to probe the rate capability of the electrolyte (*i.e.* the current densities at which the

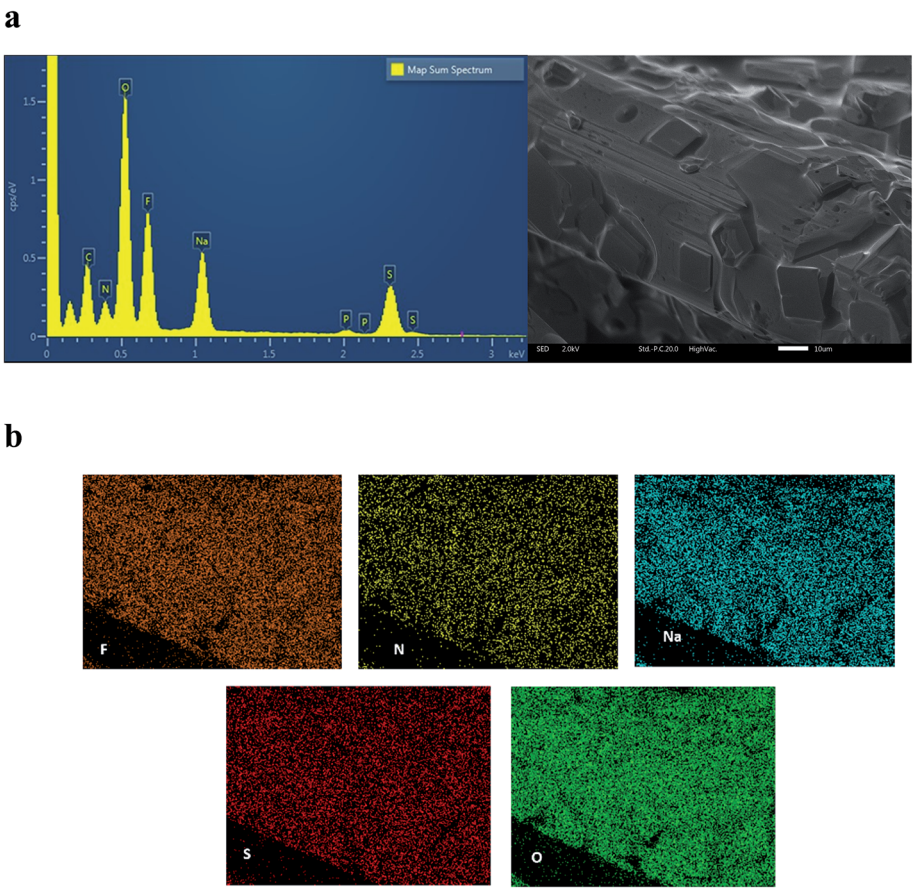

Fig. 6 (a) EDX spectrum of 90 mol% NaFSI/P_{1i444}FSI, shows high intensity of O, F and S and low intensity of C and P. (b) EDX images of 90 mol% NaFSI/P_{1i444}FSI showing the uniform distribution of FSI anion.

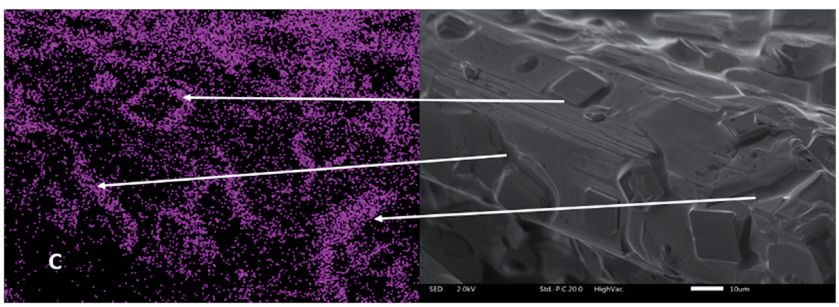

Fig. 7 The edges or holes in the right-hand image contain liquid phases. The density of C at these places is very high in the left-hand image.

sodium electrochemistry can be sustained). Moreover, to understand the interfacial stability of Na, EIS measurements were undertaken in these symmetrical cells.

Na symmetrical coin cells were constructed using an electrolyte consisting of 90 mol% of NaFSI in P_{1i444}FSI and cycled at current densities of 0.05 mA cm^{-2} (Fig. 8) and 0.1 mA cm^{-2} (Fig. S6†) at 50 °C for 10 minutes for each polarisation. Fig. 8a–c and S6† show the cycling results and also the sequential EIS spectra before polarisation and after every 10 cycles.

According to the prior work of our group on Li symmetrical cells with ionic liquids and OIPCs, a decrease in polarisation potential (also often referred to as overpotential) occurs after the few initial cycles.[4,8,9,37] However, the reduction in the polarisation potential is less substantial in the present system. This suggests that the OIPC/NaFSI mixed electrolyte presents a different chemistry and structure at the Na metal interface compared with previous systems, indicating that higher current densities/step durations may be required to initiate the electrode surface and interfacial restructuring 'pre-conditioning' process.[4] After two cycles the polarisation potential reaches 0.05 V and remains stable for the entire 80 cycles. This data shows that stripping and plating of Na metal in the sample

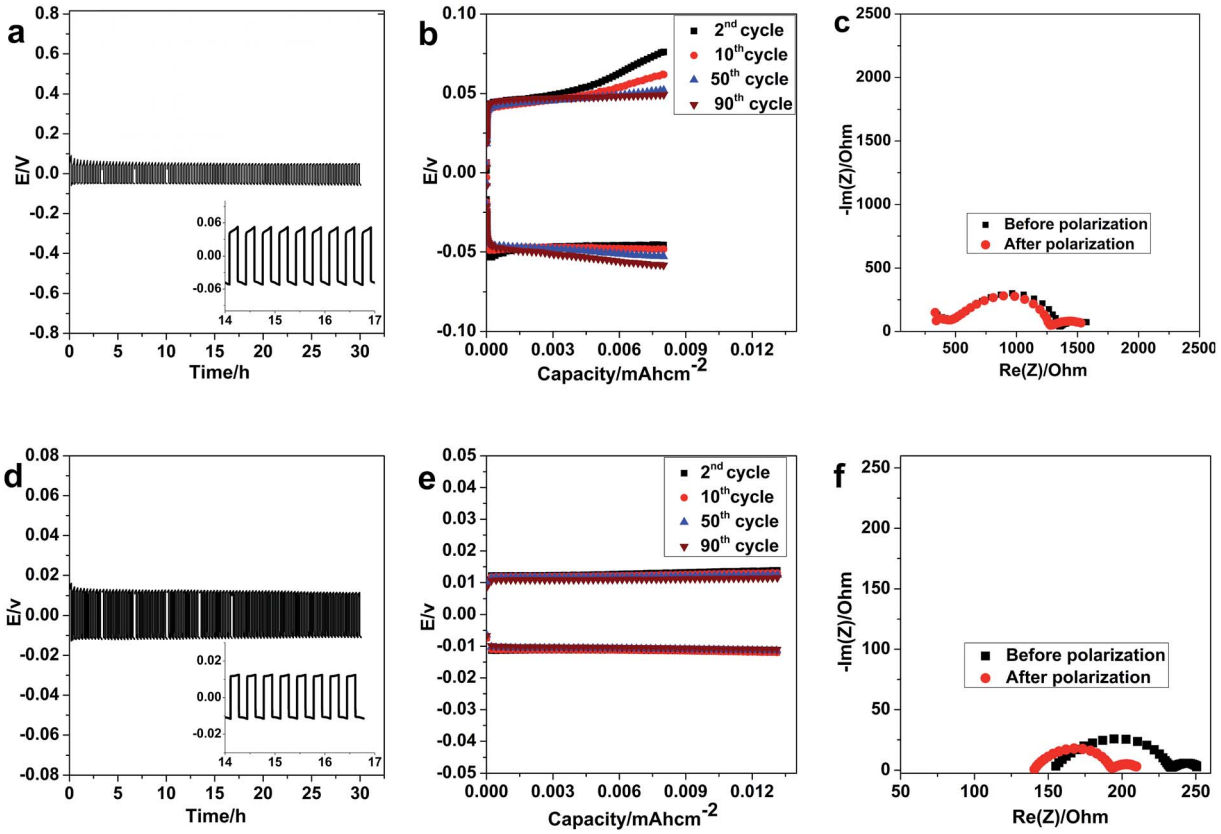

Fig. 8 (a and b) Galvanostatic cycling of 90 mol% $P_{1i444}FSI$/NaFSI, at 50 °C with a controlled current density of 0.05 mA cm^{-2} with cycling period of 10 min (c) impedance data during this experiment. (d and e) Galvanostatic cycling of 90 mol% $P_{1i444}FSI$/NaFSI at 90 °C with a current density of 0.1 mA cm^{-2} with cycling period of 10 min, (f) EIS data at 0.1 mA cm^{-2} at 90 °C.

containing a very high concentration of NaFSI is very stable. EIS data indicate a slight decrease in the internal resistance with increasing cycles.

Upon applying a higher current density (0.1 mA cm^{-2}) at 50 °C, the polarisation potential reached 1 V and remained stable during 40 cycles (Fig. S6†).

This composition was also tested at 90 °C with a current density of 0.1 mA cm^{-2} with a cycling period of 10 min (Fig. 8d–f). Under these conditions, the electrolyte operates at a very low polarisation potential. The polarisation potential reaches 0.01 V and remains stable for at least 30 hours of continuous cycling. These results demonstrate the capability of these OIPC sodium salt mixtures with an ultra-high concentration of Na salt to act as solid electrolytes for Na devices, since even at this elevated temperature the material presents as a solid.

The effect of composition on the cycling behaviour was also investigated. Fig. 9a–c presents the Na stripping and plating profiles for a 60 mol% NaFSI/40 mol% $P_{1i444}FSI$ system cycled at 0.1 mA cm^{-2} and 0.25 mA cm^{-2} with 10 minute intervals at 50 °C. The deposition and dissolution of Na is very stable throughout the whole cycling period with low and constant polarisation potentials of 0.02 and 0.05 V, respectively, when 0.1 and 0.25 mA cm^{-2} current densities were applied. A relative increase in the polarisation potential value with increasing applied current density is expected from the internal resistance of the cell.

The same experiment was undertaken at 25 °C. This results in a 10-fold increase in polarisation potential for a cell containing 60 mol% $P_{1i444}FSI$/NaFSI electrolyte at 0.1 mA cm^{-2}, as shown in Fig. 9d–f and S7c and d.†

This higher resistance at lower temperatures is expected since the conductivity of 60 mol% electrolyte at room temperature is 2×10^{-4} S cm^{-1}, whilst at 50 °C the electrolyte has more than three times higher conductivity at 7×10^{-4} S cm^{-1}. Furthermore, according to the phase diagram, the fraction of solid phase in the 60 mol% NaFSI sample at room temperature is higher than that at 50 °C. Thus, the decrease in Na-ion transport through both bulk electrolyte and interphase should be associated with a change in the composition of the electrolyte and also the morphology of the SEI layer. Another explanation for a higher total resistance of the 60 mol% NaFSI sample at room temperature might be that the lower temperature acts as a driving force for the onset of nucleation and growth of the solid phase in this material. The stripping and plating of Na metal will change the local concentration of Na at the interface, and may lead to a sufficiently high NaFSI concentration so as to promote crystallisation at this temperature. The study of the Na symmetric cell containing 90 mol% and 60 mol% of $P_{1i444}FSI$/NaFSI electrolyte indicates that the Na metal deposition/dissolution process is very stable and reversible and that Na metal can be stripped and plated at a significant rate.

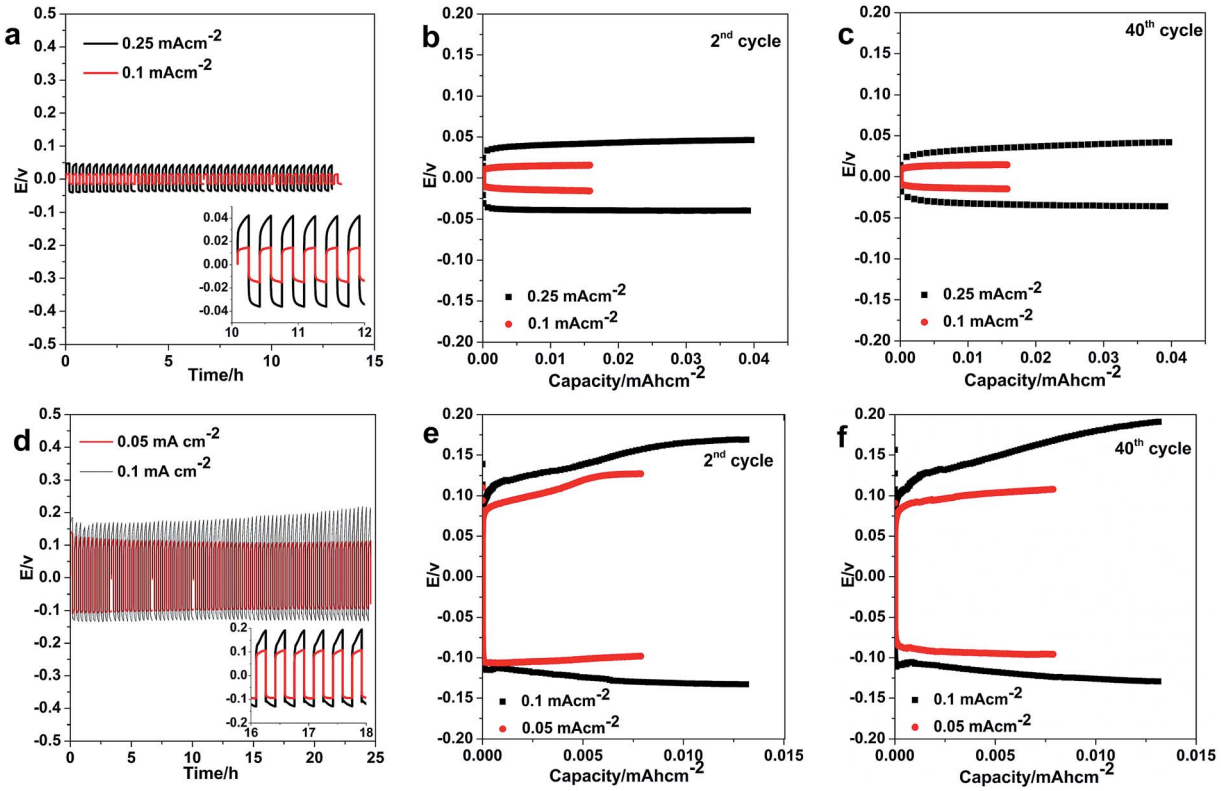

Fig. 9 (a) Galvanostatic cycling of 60 mol% $P_{1i444}FSI$/NaFSI, at 50 °C with a current density of 0.1 and 0.25 mA cm^{-2} with 10 min interval. (b) Second cycle of stripping and plating of Na. (c) 40th cycle of stripping and plating of Na. (d) Galvanostatic cycling of 60 mol% $P_{1i444}FSI$/NaFSI at room temperature with a controlled current density of 0.1 and 0.05 mA cm^{-2} with cycling period of 10 min, (e and f) second and 40th cycles of stripping and plating of Na.

3.4.2. Comparison with the previously reported $P_{111i4}NTf_2$/$NaNTf_2$ samples. For 25 mol% $P_{111i4}NTf_2$/$NaNTf_2$, the polarisation potential of the symmetric cell was around 0.05 V at 0.1 mA cm^{-2} current density for one hour at each polarisation at 50 °C. At the same current density and temperature but with 10 minutes intervals, the 60 mol% $P_{1i444}FSI$/NaFSI electrolyte showed a lower polarisation potential of around 0.02 V as is shown in Fig. S8† even though there is likely a greater proportion of solid phase in this sample (as determined from the phase diagrams). Significantly, the polarisation potential for the 60 mol% $P_{1i444}FSI$/NaFSI sample at 0.25 mA cm^{-2} is approximately the same as that for 25 mol% $P_{111i4}NTf_2$/$NaNTf_2$ at 0.1 mA cm^{-2}.

The polarisation potential of a cell containing 75 mol% $P_{111i4}NTf_2$/$NaNTf_2$, as reported in our previous work, starts at 0.1 V and increases with continued cycling (at 50 °C, 0.1 mA cm^{-2}). By comparison, the cell containing 60 mol% $P_{1i444}FSI$/NaFSI studied here exhibits much smaller and quite stable polarisation potentials at 50 °C and cycling at 0.1 mA cm^{-2} that can be illustrated from Fig. S8.† This indicates some specific role of the FSI anion in formation of the SEI layer as compared to the larger NTf_2 anions.

Interestingly, in the case of the 90 mol% NaFSI system, a lower polarisation potential (0.05 V) is observed when cycling at 50 °C and 0.05 mA cm^{-2}. This is half of that for the 75 mol% of $NaNTf_2$ sample (0.1 V) the polarisation potential of this system remained constant with cycling. Furthermore, a very low and stable polarisation potential (around 0.015 V) was recorded during 90 cycles for this high NaFSI concentration sample at 90 °C.

In comparison with 50 mol% NaFSI in C_3mpyrFSI[62] which is liquid at room temperature, 60 mol% $P_{1i444}FSI$/NaFSI provides lower polarisation potential (around 0.1 V compared to 0.2 V in the former electrolyte) at room temperature and at 0.05 mA cm^{-2}. Thus it can be seen that this new OIPC/NaFSI system shows significantly improved potential for application in a Na metal device.

3.4.3. Effect of current density. Given that previous reports for Li based OIPC[8] and ionic liquid[63] systems indicate that a preconditioning treatment can influence the polarisation potentials and stability during cell cycling, this section investigates the effect of different galvanostatic cycling regimes on cell performance. Na symmetrical coin cells were again constructed using an electrolyte of 90 mol% NaFSI in $P_{1i444}FSI$ and cycled at different current densities at both 50 °C and room temperature for 10 minutes for each polarisation. The typical voltage–time (V–t) responses at 50 °C are presented in Fig. 10. In Fig. 10a the cell has been cycled at 0.1 mA cm^{-2} and then the current density was increased to 1 mA cm^{-2} ('low-to-high') after which a current density of 0.1 mA cm^{-2} was again applied (10 cycles at each current density). A significant polarisation potential was observed at high current densities. However, the

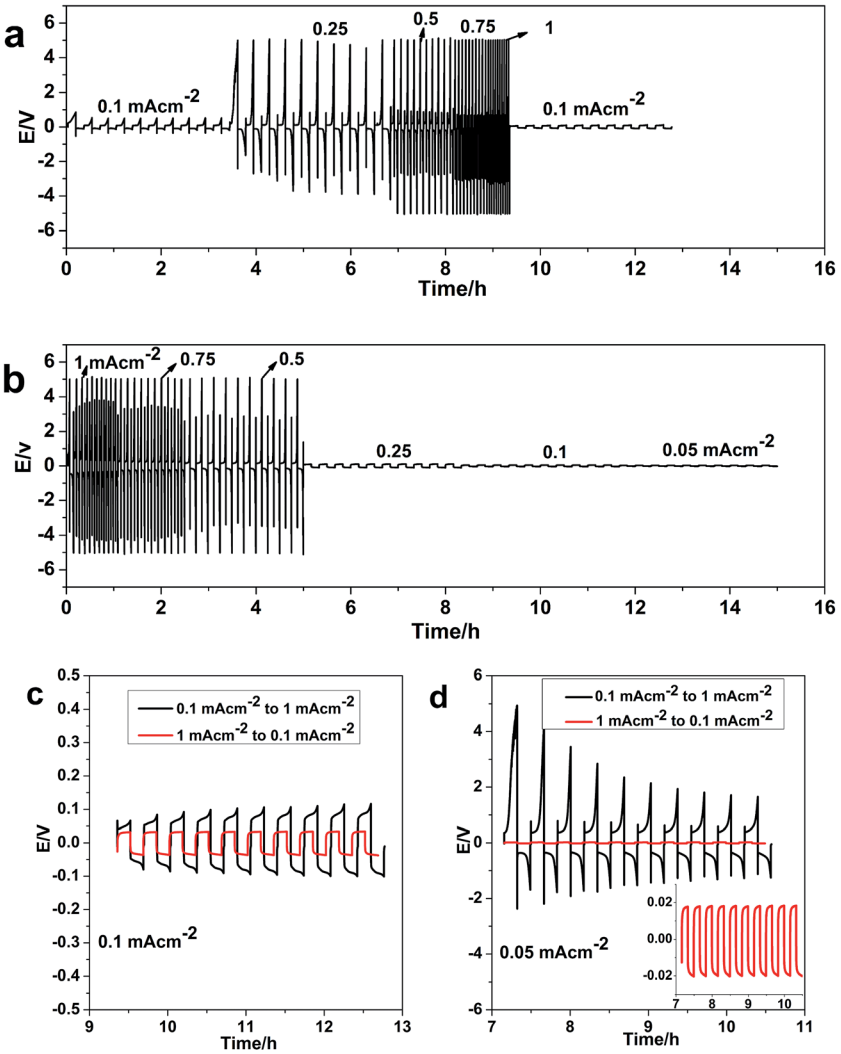

Fig. 10 Galvanostatic stripping–plating cycling of a Na|90 mol% NaFSI in $P_{1i444}FSI$|Na cell at 50 °C, (a) cycling at different current densities from 0.1 (low) to 1 (high) mA cm^{-2}, (b) cycling at different current densities from 1 (high) to 0.1 (low) mA cm^{-2}, (c) comparison between cycling results at 0.1 mA cm^{-2} after applying high to low and low to high current densities at 50 °C. (d) Comparison between cycling results at 0.05 mA cm^{-2} after applying high to low and low to high current densities at room temperature.

cell performance for the last 10 cycles (at 0.1 mA cm^{-2} current density) was improved compared to the first 10 cycles (at 0.1 mA cm^{-2} current density) prior to the pre-conditioning process. Fig. 10b shows an alternative pre-conditioning process whereby the cell was cycled from high current density to the low (1 mA cm^{-1} to 0.05 mA cm^{-2}, 'high-to-low'). In this case the polarisation potential was considerably decreased at 0.25 mA cm^{-2} compared to the low-to-high regime. Fig. 10c also shows a comparison of the cell performance at 0.1 mA cm^{-2} after the application of these two different pre-conditioning processes. Again, the high-to-low regime shows better performance. It has been previously suggested that the pre-conditioning process affects the electrode surface and SEI properties as well as the solid electrolyte through changes such as decreased grain size at the interface and increased amount of grain boundaries, leading to improved ion mobility in the interfacial region of the cycling cell.[8] More aggressive initial cycling appears to favourably modify all or some of these features to allow Na deposition/dissolution to occur at lower overpotentials in the pre-conditioned cells. More detailed impedance analysis coupled with *in situ* and *ex situ* surface analysis will be required to fully understand these effects.

4. Conclusions

The phase behaviour of $P_{1i444}FSI$ OIPC mixed with NaFSI has been explored in detail. Unusual phase behaviour was observed for salt-rich compositions ($30 < x < 60$ NaFSI), where the crystallisation process was suppressed through the increasing viscosity of the liquid phase at increasing concentration of NaFSI. The partial phase diagram allows a correlation between the thermal and physical properties at different compositions. An extensive DSC study together with conductivity measurements showed metastable behaviour at higher concentrations

of NaFSI. Furthermore, the ionic conductivity in these systems is very high at ambient temperatures, even though at high concentrations of NaFSI, the samples are predominantly in the solid state.

Sodium symmetrical cells employing the highly conductive 90 mol% NaFSI electrolyte, were constructed. They demonstrated very reversible and stable Na cycling during 80 cycles, thus confirming the applicability of these materials in Na-based electrochemical devices. Improved cycling performance was observed at higher temperatures, probably related to the higher fraction of liquid phase in the mixture. The results provide strong support for the application of these OIPC mixtures with high concentrations of Na salt as solid electrolytes. Further work is underway to characterise the behaviour in sodium cells incorporating intercalation cathodes as well as to understand the behaviour of the electrode/electrolyte interfaces.

Acknowledgements

The authors would like to express their gratitude to the ARC (Australian Research Council) for their financial support of the experimental research through Australian Laureate Fellowships FL110100013 (MF) and Fl120100019 (DRM). F. Makhlooghiazad is grateful to Deakin University for a postgraduate research scholarship. We also thankfully acknowledge funding from the ARC through DP130101652 and DP160101178. We thank Dr K. Nairn for her helpful comments and editorial assistance.

References

1 D. R. MacFarlane and M. Forsyth, *Adv. Mater.*, 2001, **13**, 957.
2 U. A. Rana, M. Forsyth, D. R. MacFarlane and J. M. Pringle, *Electrochim. Acta*, 2012, **84**, 213.
3 T. Shimizu, S. Tanaka, N. Onoda-Yamamuro, S. Ishimaru and R. Ikeda, *Faraday Trans.*, 1997, **93**, 321.
4 J. Sunarso, Y. Shekibi, J. Efthimiadis, L. Jin, J. M. Pringle, A. F. Hollenkamp, D. R. Macfarlane, M. Forsyth and P. C. Howlett, *J. Solid State Electrochem.*, 2012, **16**, 1841.
5 Y. Shekibi, T. Ruther, J. Huang and A. F. Hollenkamp, *Phys. Chem. Chem. Phys.*, 2012, **14**, 4597.
6 J. M. Pringle, P. C. Howlett, D. R. MacFarlane and M. Forsyth, *Phys. Chem. Chem. Phys.*, 2013, **15**, 1339.
7 P. Wang, S. M. Zakeeruddin, P. Comte, I. Exnar and M. Gratzel, *J. Am. Chem. Soc.*, 2003, **125**, 1166.
8 L. Jin, P. C. Howlett, J. Efthimiadis, M. Kar, D. R. Macfarlane and M. Forsyth, *J. Mater. Chem.*, 2011, **21**, 10171.
9 L. Jin, P. C. Howlett, J. M. Pringle, J. Janikowski, M. Armand, D. R. Macfarlane and M. Forsyth, *Energy Environ. Sci.*, 2014, **7**, 3352.
10 P. C. Howlett, J. Sunarso, Y. Shekibi, E. Wasser, L. Jin, D. R. MacFarlane and M. Forsyth, *Solid State Ionics*, 2011, **2**, 73.
11 J. M. Pringle, J. Adebahr, D. R. Macfarlane and M. Forsyth, *Phys. Chem. Chem. Phys.*, 2010, **12**, 7234.
12 Q. Li, X. Chen, J. Zhao, L. Qiu, Y. Zhang, B. Sun and F. Yan, *J. Mater. Chem.*, 2012, **22**, 6674.
13 M. Yoshizawa-Fujita, K. Fujita, M. Forsyth and D. R. MacFarlane, *Electrochem. Commun.*, 2007, **9**, 1202.
14 Z.-B. Zhou and H. Matsumoto, *Electrochem. Commun.*, 2007, **9**, 1017.
15 U. A. Rana, P. M. Bayley, R. Vijayaraghavan, P. C. Howlett, D. R. Macfarlane and M. Forsyth, *Phys. Chem. Chem. Phys.*, 2010, **12**, 11291.
16 M. Volel, P. J. Alarco, Y. Abu-Lebdeh and M. Armand, *ChemPhysChem*, 2004, **5**, 1027.
17 D. R. MacFarlane, P. Meakin, J. Sun, N. Amini and M. Forsyth, *J. Phys. Chem. B*, 1999, **103**, 4164.
18 M. Moriya, T. Watanabe, W. Sakamoto and T. Yogo, *RSC Adv.*, 2012, **2**, 8502.
19 D. R. MacFarlane, J. Huang and M. Forsyth, *Nature*, 1999, **402**, 792.
20 Y. Abu-Lebdeh, A. Abouimrane, P.-J. Alarco and M. Armand, *J. Power Sources*, 2006, **154**, 255.
21 Y. Abu-Lebdeh, P.-J. Alarco, A. Abouimrane, L. Ionescu-Vasii, A. Hammami and M. Armand, *J. New Mater. Electrochem. Syst.*, 2005, **8**, 197.
22 P. J. Alarco, Y. Abu-Lebdeh, N. Ravet and M. Armand, *Solid State Ionics*, 2004, **172**, 53.
23 W. A. Henderson, D. M. Seo, Q. Zhou, P. D. Boyle, J.-H. Shin, H. C. De Long, P. C. Trulove and S. Passerini, *Adv. Energy Mater.*, 2012, **2**, 1343.
24 H. Ishida, N. Matsuhashi, R. Ikeda and D. Nakamura, *J. Chem. Soc. Faraday Trans.*, 1989, **85**, 111.
25 A. Hill, J. Huang, J. Efthimiadis, P. Meakin, M. Forsyth and D. MacFarlane, *Solid State Ionics*, 2002, **154**, 119.
26 S. J. Pas, J. Huang, M. Forsyth, D. R. MacFarlane and A. J. Hill, *J. Chem. Phys.*, 2005, **122**, 064704.
27 J. M. Pringle, P. C. Howlett, D. R. MacFarlane and M. Forsyth, *J. Mater. Chem.*, 2010, **20**, 2056.
28 Y. Abu-Lebdeh, P. J. Alarco and M. Armand, *Angew. Chem.*, 2003, **42**, 4736.
29 A. J. Seeber, M. Forsyth, C. M. Forsyth, S. A. Forsyth, G. Annat and D. R. MacFarlane, *Phys. Chem. Chem. Phys.*, 2003, **5**, 2692.
30 S. J. Pas, J. M. Pringle, M. Forsyth and D. R. MacFarlane, *Phys. Chem. Chem. Phys.*, 2004, **6**, 3721.
31 Y. Shekibi, A. Gray-Weale, D. R. MacFarlane, A. J. Hill and M. Forsyth, *J. Phys. Chem. C*, 2007, **111**, 11463.
32 Y. Shekibi, S. J. Pas, N. M. Rocher, B. R. Clare, A. J. Hill, D. R. MacFarlane and M. Forsyth, *J. Mater. Chem.*, 2009, **19**, 1635.
33 T. Chimdi, D. Gunzelmann, J. Vongsvivut and M. Forsyth, *Solid State Ionics*, 2015, **272**, 74.
34 J. Janikowski, C. Forsyth, D. R. MacFarlane and J. M. Pringle, *J. Mater. Chem.*, 2011, **21**, 19219.
35 W. A. Henderson, V. G. Young, S. Passerini, P. C. Trulove and H. C. De Long, *Chem. Mater.*, 2006, **18**, 934.
36 W. A. Henderson, M. Herstedt, V. G. Young, S. Passerini, H. C. De Long and P. C. Trulove, *Inorg. Chem.*, 2006, **45**, 1412.
37 P. C. Howlett, Y. Shekibi, D. R. MacFarlane and M. Forsyth, *Adv. Energy Mater.*, 2009, **11**, 1044.
38 D. R. MacFarlane, M. Forsyth, P. C. Howlett, M. Kar, S. Passerini, J. M. Pringle, H. Ohno, M. Watanabe, F. Yan,

W. Zheng, S. Zhang and J. Zhang, *Nat. Rev. Mater*, 2016, **1**, 15005.
39 P.-J. Alarco, Y. Abu-Lebdeh and M. Armand, *Solid State Ionics*, 2004, **175**, 717.
40 K. Tsunashima and M. Sugiya, *Electrochem. Commun.*, 2007, **9**, 2353.
41 K. J. Fraser and D. R. MacFarlane, *Aust. J. Chem.*, 2009, **62**, 309.
42 V. Armel, D. Velayutham, J. Sun, P. C. Howlett, M. Forsyth, D. R. MacFarlane and J. M. Pringle, *J. Mater. Chem.*, 2011, **21**, 7640.
43 K. Yoshii, K. Yamaji, T. Tsuda, K. Tsunashima, H. Yoshida, M. Ozaki and S. Kuwabata, *J. Phys. Chem. B*, 2013, **117**, 15051.
44 F. Makhlooghiazad, D. Gunzelmann, M. Hilder, D. R. MacFarlane, M. Armand, P. C. Howlett and M. Forsyth, *Adv. Energy Mater.*, 2016, 1601272.
45 C. Michot, M. Armand, M. Gauthier and N. Ravet, *US Pat.*, 6365301B1, 2002.
46 S. Seki, Y. Kobayashi, H. Miyashiro, Y. Ohno, Y. Mita and N. Terada, *J. Phys. Chem. C*, 2008, **112**, 42.
47 A. I. Bhatt, A. S. Best, J. Huang and A. F. Hollenkamp, *J. Electrochem. Soc.*, 2010, **157**, A66.
48 M. Ishikawa, T. Sugimoto, M. Kikuta, E. Ishiko and M. Kono, *J. Power Sources*, 2006, **162**, 658.
49 E. Paillard, Q. Zhou, W. A. Henderson, G. B. Appetecchi, M. Montanino and S. Passerini, *J. Electrochem. Soc.*, 2009, **156**, A891.
50 A. I. Bhatt, A. S. Best, J. Huang and A. F. Hollenkamp, *J. Electrochem. Soc.*, 2010, **157**, A66.
51 A. Budi, A. Basile, G. Opletal, A. F. Hollenkamp, A. S. Best, R. J. Rees, A. I. Bhatt, A. P. O'Mullane and S. P. Russo, *J. Phys. Chem. C*, 2012, **116**, 19789.
52 M. Forsyth, G. Girard, A. Basile, D. R. Macfarlane, F. Chen and P. C. Howlett, *Electrochim. Acta*, 2016, **220**, 609–617.
53 P. J. Timmermans, *J. Phys. Chem. Solids*, 1961, **18**, 1.
54 W. A. Henderson, *J. Phys. Chem. B*, 2006, **110**, 26.
55 S. D. Han, O. Borodin, D. M. Seo, Z. B Zhou and W. A. Henderson, *J. Electrochem. Soc.*, 2014, **161**, A2042.
56 Q. Zhou, K. Fitzgerald, P. D. Boyle and W. A. Henderson, *J. Chem. Mater.*, 2010, **22**, 3.
57 Q. Zhou, W. A. Henderson, G. B. Appetecchi and S. Passerini, *J. Phys. Chem. C*, 2010, **114**, 13.
58 C. Ding, T. Nohira, K. Kuroda, R. Hagiwara, A. Fukunaga, S. Sakai, K. Nitta and S. Inazawa, *J. Power Sources*, 2013, **238**, 296.
59 E. Paillard, Q. Zhou, W. A. Henderson, G. B. Appetecchi, M. Montanino and S. Passerini, *J. Electrochem. Soc.*, 2009, **156**, A891.
60 D. Monti, E. Jónsson, M. R. Palacín and P. Johansson, *J. Power Sources*, 2014, **245**, 630.
61 S. A. Mohd Noor, P. C. Howlett, D. R. MacFarlane and M. Forsyth, *J. Electrochim Acta*, 2013, **114**, 766.
62 M. Forsyth, H. Yoon, F. Chen, H. Zhu, D. R. MacFarlane, M. Armand and P. C. Howlett, *J. Phys. Chem. C*, 2016, **120**, 4276.
63 A. Basile, A. I. Bhatt and A. P. O Mullane, *Nat. Commun.*, 2016, **7**, 11794.